The International Journal of Advanced Manufacturing Technology (2023) 125:3135–3148
https://doi.org/10.1007/s00170-023-10843-1

ORIGINAL ARTICLE

Assessment of the surface integrity of AISI H13 tool steel after milling with carbide and cermet inserts

Michele Lisboa Silveira[1] · Diogo Azevedo de Oliveira[2] · Anderson Júnior dos Santos[2] · Paulo Eustáquio de Faria[1] · Alexandre Mendes Abrão[2]

Received: 30 September 2022 / Accepted: 5 January 2023 / Published online: 30 January 2023

Abstract

The present work investigated the influence of face milling parameters (cutting speed, feed per tooth and depth of cut) and tool grade (tungsten carbide and cermet) on the surface integrity of annealed AISI H13 steel in terms of components of resultant force, machined surface temperature, surface quality and induced residual stresses. The results indicated that depth of cut and feed per tooth were the parameters responsible for the highest milling force components; furthermore, the milling force components did not depend on the cutting speed cutting tool grade. Depth of cut was the only factor that influenced the temperature on the machined surface, indicating that an increase in this parameter raises the temperature considerably. Regarding the machined surface quality, feed per tooth was the main factor influencing the roughness parameters for both tool materials, while the influence of tool grade, cutting speed, depth of cut was negligible. The tribological effect of the lubricating-cooling action of the cutting fluid on chip-tool and workpiece-tool interfaces was beneficial to the improvement of the surface quality. Surface roughness was significantly better after milling with the cermet in comparison with tungsten carbide under the same cutting conditions. Tensile residual stresses prevailed in the layer immediately below the surface, which may represent unfavorable conditions for the performance of the component. In general, high cutting speed associated with high feed per tooth, low depths of cut and cutting fluid application induced tensile residual stress of lower intensity. Finally, cutting tool grade did not affect the residual stresses remarkably.

Keywords Milling · Milling force · Milled surface temperature · Roughness · Residual stresses

1 Introduction

The AISI H13 is a hot work die steel with wide industrial application in mould and dies manufacture due to its low plasticity, high hardness, low extensibility and ability to achieve low surface roughness in machining operations, elevated wear resistance, even when used at high temperatures and for long periods [1, 2]. AISI H13 steel behaves differently at different hardness levels, thus affecting the machining force and the overall process behavior [3]. Therefore, the need to minimize cutting force and energy consumption during machining in order to reduce the mechanical and thermal stresses is required [4], since the increase of the machining force can lead to the instability of the process, resulting in excessive vibrations and temperature increase. Therefore, an appropriate choice of tool, cutting parameters and cooling environments enable the control of milling forces, ensuring the integrity of the milled product. Cui et al. [5] performed milling of AISI H13 steel and found that the machining force increases proportionally to the cutting speed. The authors explain that the increase in cutting speed promotes the elevation of temperatures, leading to an adherence of material on the tool rake face, increasing the coefficient of friction and, consequently, the increase of forces. Ding et al. [6] investigated the effects of cutting parameters on cutting forces in hard milling of AISI H13 steel with carbide coated tools and identified that depth of cut and feed per tooth are the two dominant cutting parameters responsible for increased cutting forces due to an increase in chip

✉ Michele Lisboa Silveira
michelesilveira1991@gmail.com

[1] Industrial Engineering Graduate Program, Universidade Federal de Minas Gerais, Av. Antônio Carlos, 6627. Campus Pampulha, Belo Horizonte, 31270-901, Minas Gerais, Brazil

[2] Mechanical Engineering Graduate Program, Universidade Federal de Minas Gerais, Av. Antônio Carlos, 6627. Campus Pampulha, Belo Horizonte, 31270-901, Minas Gerais, Brazil

cross-section. Afazov et al. [3] analyzed the cutting forces when micromilling AISI H13 steel at hardness between 35 and 60 HRC. The authors found that cutting forces and cutting temperatures increase with increasing AISI H13 hardness, while process stability limits decrease with increasing hardness.

When applied in molds and dies, AISI H13 steel must meet high surface topography requirements and roughness is one of the main methods for assessing surface quality [6]. Roughness parameters are widely used as an index of product quality and are related to aesthetics criteria, corrosion resistance, processing advantages, tribological aspects, fatigue life, as well as enabling improvement and precise fit for critical contact surfaces [7]. Do, Nguyen and Phan [8] evaluated the roughness after milling AISI H13 and concluded that the roughness depends of cooling conditions and cutting parameters. The authors concluded that using cutting fluid and minimum values for feed per tooth and depth of cut were responsible for the reduction in surface roughness.

The measurement and analysis of temperature in milling process is of utmost importance in order to preserve the surface integrity of the part. When the surface of a workpiece is regularly exposed to thermal cycling (heating and cooling), a temperature gradient arises, resulting in thermal stresses along the layers adjacent to the surface that contribute to the propagation of surface nucleated cracks. As the depth increases from the surface, the effect of thermal cycling decreases, ceasing crack propagation [9]. Li et al. [10] report that the combination of localized, high-intensity thermomechanical effects that occur during hard milling involves severe plastic deformation, grain refinement, and phase transformation. According to the authors, phase transformation always occurs and is detrimental to surface integrity, inducing work hardening and white layer formation. However, not all techniques are effective or simple to apply [11]. Some difficulties that can be found in the measurement processes, such as establishing the appropriate environmental conditions and the emissivity of the analyzed material [12, 13]. The method used to estimate the milled surface temperature ABNT H13 steel of this work was proposed by Moreira et al. [14], who compared two different methods: the first was based on the diffuse-grey approximation, with a constant emissivity value, and the second used directional-spectral radiative heat transfer relationships, which is suitable for opaque surfaces with emissivity approximately constant in relation to wavelength, but is not ideal for measuring temperature in milling AISI H13. The second is the methodology of the directional-spectral radiative heat transfer relationships, which showed a satisfactory agreement with the temperature values reported in the literature.

The performance of machined components is associated with the residual stresses induced during the process, which affect the fatigue life, corrosion resistance and distortion of the parts [15]. Residual stresses may arise from thermal and mechanical effects and can be beneficial when their nature is compressive, or detrimental when it is tensile. Teppernegg et al. [16] evaluated the residual stresses in coated carbide inserts after milling a 42CrMo4 steel and found that the residual stresses and wear of the inserts were mainly influenced by mechanical and thermal shocks. Shaw [17] asserts that a region of the workpiece ahead of the cutting tool (before actual cutting) concentrates compressive residual stresses and a large amount of strain energy is stored. After cutting, this stored energy associated with the compressive stresses can be released and converted into a tensile energy. However, if the compressive residual stress is high enough and the stored energy is quickly released due to a high cutting speed immediately after the tool passes over the machined surface, the compressive residual stress is converted into a tensile residual stress.

Cutting tool material is another parameter that can affect the surface integrity of the part due to the tribological aspects. Aslan and Camuscu [18] state that cubic boron nitride tools achieved longer tool life and produced a better surface finish on the workpiece when compared with coated carbide, mixed alumina and coated cermet when milling AISI H13 steel. This result is due to the lower tool wear promoted by the CBN tool coating. Ribeiro et al. [19] compared coated carbide and cermet inserts when milling AISI H13 steel and did not find a significant difference between the cutting tool grades tested in terms of dimensional deviation.

According to Kun and Wenyu [20], most research on surface integrity is limited to observing the variation in residual stresses when the cutting parameters, such as cutting speed, feed rate, depth of cut and tool geometry are changed. However, there are other variables that can affect residual stresses and that are difficult to measure accurately, therefore, they are often neglected, such as the influence of different cutting tools materials, the behavior of the machining force components, cutting temperature and surface finish. In applications such as molds and dies, it is important to ensure the surface integrity of the AISI H13 steel after milling. For this reason, low surface roughness is required aimed at negligible stress concentration and neutral or low tensile residual stresses near the surface, since stresses of this nature tend to lead to crack propagation and reduce fatigue life. Therefore, the main purpose of this research is to correlate the mechanical and thermal effects induced by the input parameters on the responses and their relationship with the surface integrity of milled AISI H13 steel. The mechanical effects induced by high milling

forces can adversely affect the surface quality by generating forced vibrations and/or intense plastic deformation on the surface, while thermal effects resulting from excessive heat generation can induce tensile residual stresses of higher intensity and impair the fatigue life of the component. Therefore, it is intended to establish a correlation between the input parameters (cutting speed, feed per tooth, depth of cut, cutting tool material and use of cutting fluid) and the response variables (milling force components, machined surface temperature, roughness and residual stresses) that allow the better understanding of the behavior of this material when subjected to the cyclic mechanical and thermal loads and to identify favorable cutting conditions associated with superior surface integrity of the machined part.

2 Materials and methods

AISI H13 hot work die steel was selected as work material and subjected to annealing in order to homogenize the specimens and ensure that they were free from residual stresses. The heat treatment consisted of uniformly heating up to a temperature of 690ºC and keeping the specimens at this level for 3.5 h in a furnace with a controlled atmosphere to avoid decarburization. After this period, the temperature was reduced to 480 ºC, followed by cooling in the furnace to room temperature. After heat treatment, the average hardness of the AISI H13 steel specimens was 178 ± 8 HV.

Milling tests were performed on a machining center with power of 9 kW and maximum speed of 7000 rpm. The milling cutter used was a 50-mm diameter face mill with three inserts and the approach angle of 45° (Sandvik Coromant ASX 445-050A03R). Two cutting tool grades were employed: ISO grade P20 tungsten carbide (WC) (Mitsubishi Carbide SEMT13T3AGSN-JM MP 6120) and cermet (Mitsubishi Carbide SEMT13T3AGSN-JM NX4545).

A Kistler piezoelectric dynamometer model 9272 connected to National Instruments USB – 6366 data acquisition system and to a Kistler amplifier (type 5073) was used to acquire the feed force (Fx), thrust force (Fy) and tangential force (Fz), where *x*, *y*, and *z* represent the axis directions. Force signals were acquired using ManuWare and NI LabView SignalExpress software at an acquisition rate of 1 kHz.

A FLIR thermographic camera model SC 660 with a 19-mm lens was used to measure the specimens surface temperature during the milling tests. Temperature was collected only when dry cutting, because the thermographic camera cannot be exposed to the cutting fluid (harmful to its components). The camera was positioned on a tripod at a distance of 260 mm form the specimens and at a tilt angle of 37° and pointed at the workpiece surface. In order to obtain a better access to the cut region by the camera, the temperature measurements were carried out in the up milling direction. The temperature measurement range was from 0 to 500 °C and the acquisition rate was 15 Hz. The thermogram files for each test were processed in FLIR Quick Report 1.2 SP2 software. The methodology and calculation routine for acquiring the milled surface temperature during milling of AISI H13 steel can be found elsewhere [14].

Surface topography was assessed on a Hommel Etamic T8000 contact profilometer with a Tku 300/600 pick-up and diamond stylus with 90º and the tip radius of 5 µm. MountainsMap software was used to generate the images of the primary surfaces and process the following roughness parameters: arithmetical mean deviation (Ra), root mean square deviation (Rq), ten points height of the roughness profile (Rz) total height of the profile (Rt).

The hole-drilling method was used to acquire the microstrains and calculate the residual stresses according to ASTM E837-13a [21] standard. After cleansing each specimen, a rosette model PA 06 060 RF 120L was attached to the milled surface. The fixed strain gauges were identified in order to obtain the microstrains corresponding, respectively, to the *X* axis (parallel to the feed direction), *Z* and *Y* axes (microstrains perpendicular to the feed direction). After fixing the rosette, the terminals were connected to a Vishay P3 microstrain indicator and recorder. Subsequently, a RS–200 milling guide high-speed turbine was positioned and the hole was produced using a Jet FG 38 inverted conical carbide drill (maximum diameter of 1.59 mm) at a speed of 210,000 rpm. The hole was drilled to a depth of 1 mm and drilled in 20 steps using 0.05-mm increments. After performing the 20 increments, the microstrains data were processed by the Vishay Hdrill software. According to El-Khabeery and Fattouh [22], residual stress curves usually start from an absolute maximum value below the surface and then stabilize at values close to zero after a certain depth. It was observed that the residual stresses reached at zero at a depth of 225 µm below the surface for all tested conditions, therefore, the results are given up to this value. Figure 1(a) shows the milling setup and Fig. 1(b) shows the setup to measure strains.

To determine the experimental design for this research, a study was conducted considering different decision-making methods for determining optimal parameters. Any engineering process has a decision-making component to which is usually associated with effort and cost reduction [23]. Most machining studies use the Taguchi

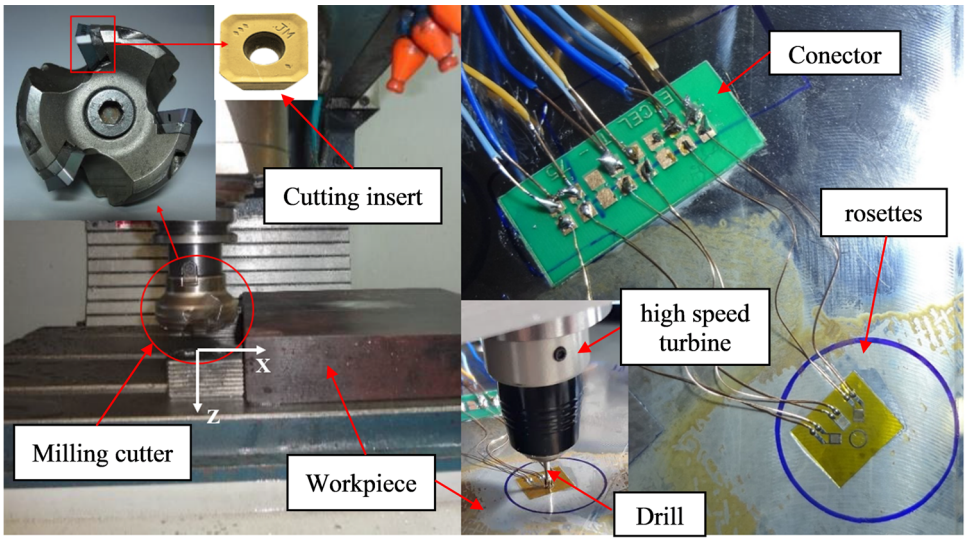

Fig. 1 Milling setup of the (a) tool and workpiece assembly (b) rosette and connector attached on the milled surface

method [24]; however, this method is not reliable when the required responses are associated with industrial applications [25], since the individual factors considered in the Taguchi method may have different optimal solutions. The Technique for Order of Preference by Similarity to Ideal Solution (TOPSIS) is a decision-making method with multi-attribute characteristics used to determine the optimal alternatives from a limited selection [26, 27]. In this method, an optimized solution can be found, thus reducing the uncertainty in the determination of the input parameters when the machining process is executed. Alternatively, Response Surface Methodology (RSM) is a statistical approach in which the responses of experiments are formulated as a function of input parameters, as reported by Ramnath and Thyla [25], who also developed a guide method in determining response values by varying machining conditions, thus providing the formulation of a functional relationship between input parameters and measured responses. Also noteworthy is the analytical hierarchy procedure (AHP) method, which aims to select the optimal milling condition in order to understand the responses of the machining operation, such as thrust force, tangential force and surface, and roughness [28].

The experimental design methods presented above are effective in decision-making; however, many of these methods require a large number of experiments, considerably increasing the time and cost of operations and analysis, making it unfeasible in specific cases, such as measurements of residual stresses. If interactions can be assumed to be insignificant, information about the main effects can be obtained by running only a fraction of the experimental design. Thus, Plackett-Burman stands out as a fractional experiment that can be applied when many factors are considered and the aim is to identify the most important factors early in the experimentation phase [29].

Plackett-Burman is the experimental design used in this work. This design is classified as a two-level fractional factorial design or 2k design, and, as a rule, must be designed with parameters up to k (where $k = N - 1$ and N the total number of runs) [30]. These experiments can be used for N = 12, 20, 24, 28 and 36. The designed arrangements are multiples of four, composed of positive sign for the higher level (represented by +1), and negative sign for the lower level (represented by −1). When a center points is added, the sign is considered to be 0 [29]. The experimental work was designed using Minitab 17 software and the factors, cutting speed (v_c), feed per tooth (f_z), depth of cut (a_p) and cutting fluid (CF), were tested randomly. In addition, two test designs were performed to evaluate the effects of both cutting tool materials: tungsten carbide (WC) and cermet. Since the Plackett-Burman is a 2k-type design, i.e. it only allows the factors to vary on two levels, the center point is added for the numerical parameter. The central point represents an intermediate value between the lower and upper levels for the parameters used [31]. For the present work, the central points are as follows: v_c = 150 m/min, f_z = 0.10 mm/rev and a_p = 1 mm. The addition of the center point in a two-level factorial design enables detecting curvature in the fitted data. The existence of a curvature indicates that the average response at the center point is higher or lower than the average response at the extreme levels. Therefore, a Plackett-Burman design was performed with 12 tests, replication at the center point, resulting in 16 tests for each cutting tool grade. Table 1 presents the milling parameters and their levels used for tungsten carbide (WC) and cermet tools.

Table 1 Milling parameters

Parameters	Values		
	Lower level (-1)	Central point (0)	Higher level (+1)
Cutting speed, v_c (m/min)	100	150	200
Feed per tooth, f_z (mm/rev)	0.05	0.10	0.15
Depth of cut, a_p (mm)	0.5	1.0	1.5
Cooling environment	Cutting fluid	–	Dry cutting

3 Results and discussion

3.1 Components of the milling force

The components of the milling force are presented in Fig. 2: feed force (Fx), thrust force (Fy) and tangential force (Fz).

The analysis of variance indicated that neither cutting speed nor the application of cutting fluid significantly affected the components of the milling force (p-value < 0.05). Moreover, depth of cut presented the largest percentage contribution to the three force components. According to Fig. 2(a) and (b), increasing depth of cut and/or feed per tooth, respectively, raised the components of the milling force for both WC and cermet tools. This behavior was reported by [6, 32] and can be explained by the fact that, increasing depth of cut and/or feed per tooth implies in a larger chip cross section, thus requiring higher forces to remove material. In addition, the higher the depth of cut and feed per tooth, the larger the chip-tool contact area and, consequently, the adhesion of the chip on the rake face [33] and the components of the milling force [34]. The response of the milling force components at the center point for both feed per tooth (f_z = 0.10 mm/rev) and depth of cut (a_p = 1.0 mm) was not higher or lower than the mean value at the extreme levels (f_z = 0.05 mm/rev and 1.5 mm/rev and a_p = 0.5 and 1.5 mm); therefore, it can be concluded that the

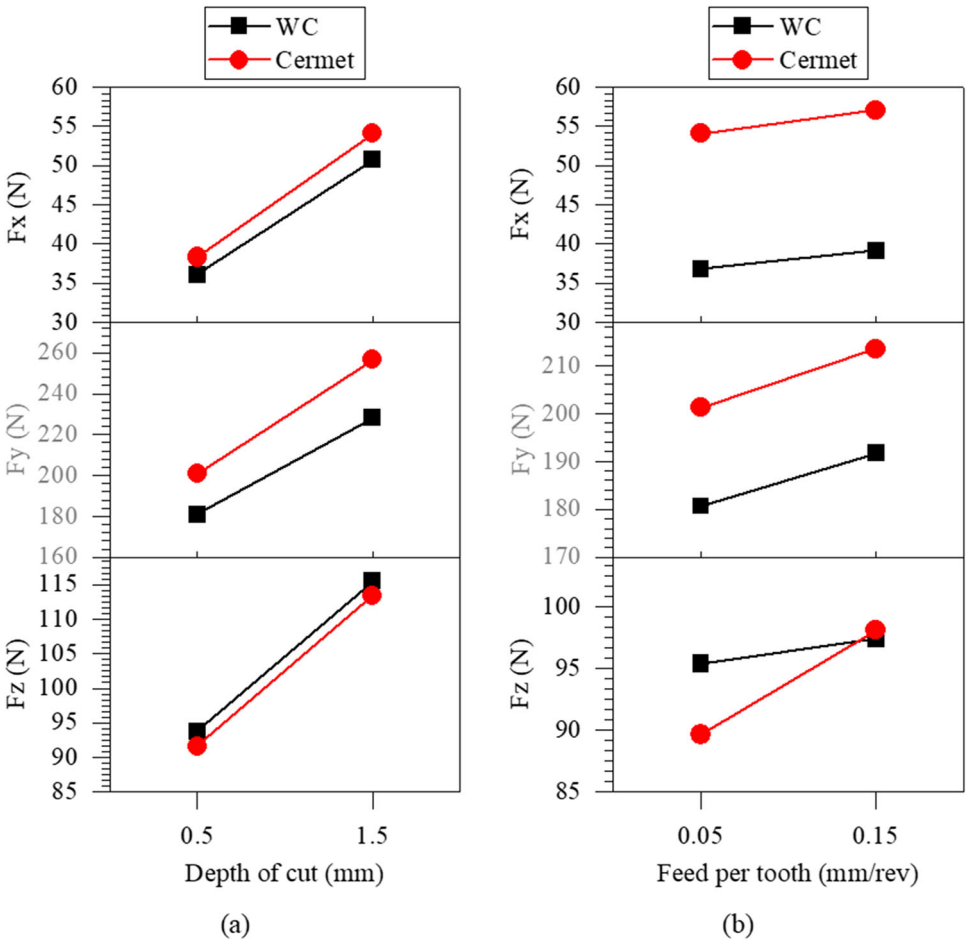

Fig. 2 Effect of (a) depth of cut and (b) feed per tooth on the components of the milling force

studied factors did not present a curved relationship with the responses.

The Fy component presented the highest value (followed by Fz and Fx) for both depth of cut and feed per tooth. This behavior was observed for the WC and cermet inserts and can be explained by the fact that all the tests were conducted for down milling; thus, promoting generates a lower force for the *X* axis component, which is parallel to the feed direction. The *Y* axis component presented the highest values because of its location perpendicular to the feed direction, requiring more effort for material removal. Finally, the *Z* axis component presented an intermediate value because it is not associated with material removal.

The two-sample *t*-test performed to compare the Fx, Fy and Fz values generated by the WC and cermet inserts gave *p*-values of 0.781; 0.653 and 0.801; respectively. Since the *p*-value was greater than 0.05, the null hypothesis must be accepted, i.e. the difference between the average forces in the three axes generated by the WC inserts compared to the cermet inserts is not statistically significant. Thus, if the aim of the milling operation is to minimize the components of the force, low levels of depth of cut and feed per tooth are indicated since these parameters were predominant. In contrast, a high cutting speed can be employed to maximize production and the use of cutting fluid can be suppressed.

3.2 Milled surface temperature

The *t*-tests performed to determine the influence of investigated factors on the milled surface temperature indicated that depth of cut was the only parameter which affected the temperature of the milled surface. When cutting speed, feed per tooth and tool material were changed, the scatter in the box-plots did not allow to assert that within the range tested, these parameters statistically affected the surface temperature (no difference between the mean values of the temperature under the different levels of the evaluated parameters). Although the elevation of cutting speed and feed per tooth is likely to increase the temperature in the chip-tool interface (as well as the use of a cutting tool material with lower thermal conductivity), a significant part of the heat generated is conducted away from the cutting zone by the chip and an appreciable increase in the machined surface temperature is not detected by the infrared camera. Despite the remarkable advantage of being a non-intrusive technique, the fact that the thermal radiation method is not capable of measuring the interface temperature in oblique cutting remains a major drawback.

Figure 3(a) shows that increasing the depth of cut significantly raises the milling temperature on the surface, as was also noted by Yan, Hua and Shivpuri [35]. This

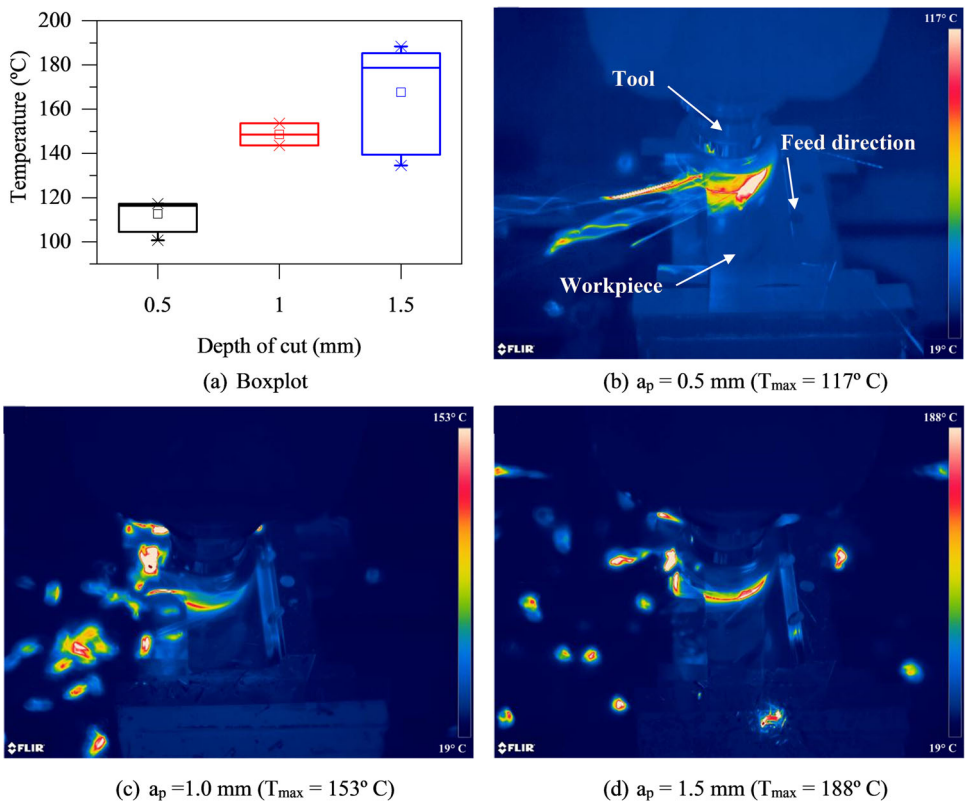

(a) Boxplot

(b) a_p = 0.5 mm (T_{max} = 117º C)

(c) a_p =1.0 mm (T_{max} = 153º C)

(d) a_p = 1.5 mm (T_{max} = 188º C)

Fig. 3 Milled surface temperature: (a) influence of depth of cut, thermograms for milling with (b) a_p = 0.5 mm, (c) a_p = 1.0 mm and (d) a_p = 1.5 mm

Table 2 *P*-values for the roughness parameters

	Ra		Rq		Rt		Rz	
Parameters	WC	Cermet	WC	Cermet	WC	Cermet	WC	Cermet
v_c (m/min)	0.056	0.736	0.175	0.532	0.239	0.096	0.097	0.390
f_z (mm/rev)	**0.001**	**0.001**	**0.008**	**0.002**	**0.002**	0.140	**0.004**	**0.014**
a_p (mm)	0.951	0.793	0.307	0.172	0.841	0.140	0.538	0.241
Cutting fluid	0.079	**0.009**	0.079	**0.009**	0.362	**0.009**	0.157	**0.002**
Curvature	0.155	0.837	0.688	0.369	0.737	0.821	0.860	0.584

behavior can be explained due to the increase of the chip cross-section, which increases the energy required to perform the cut [3]. Consequently, higher forces (Fig. 2(a)) and higher temperatures are expected when the axial depth of cut is elevated. Figure 3(b) to (d) show the thermograms used to identify the temperature distribution on the machined surface as a function of depth of cut during dry milling. The lowest temperature was obtained for an axial depth of cut of 0.5 mm (Fig. 3(b)), and reached 117°C. Small areas at low temperatures are observed. The white regions near the cutting zone, still at low temperature, are chips in formation. Increasing the axial depth of cut to1 mm elevated the temperature by approximately 31%, reaching 153°C (Fig. 3(c)). The region of the highest temperature is identified at the chip exit when the up milling direction.

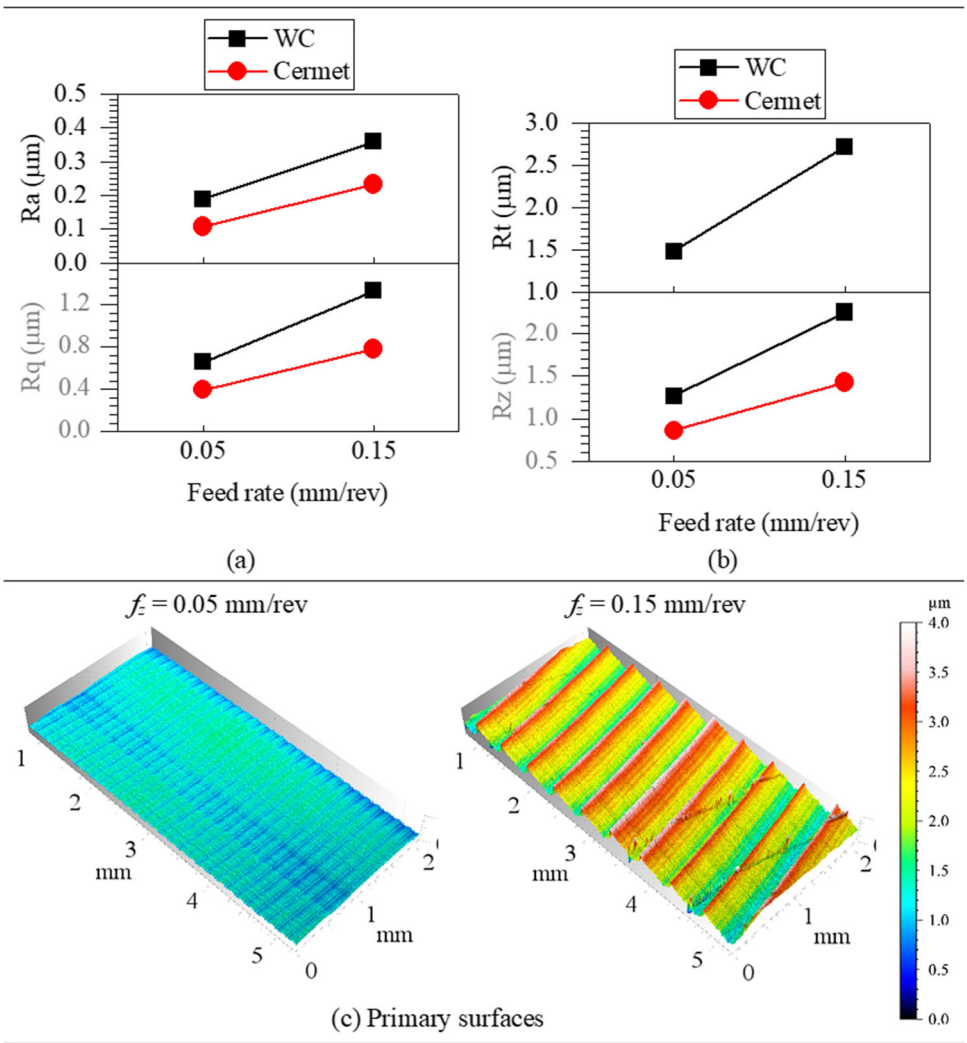

Fig. 4 Influence of feed per tooth on the roughness parameters: (a) Ra and Rq, (b) Rt and Rz and (c) primary surfaces for v_c = 100 mm/min, a_p = 1.5 mm and Tool = WC

According to the analytical model developed by Tadić, Marjanović and Mitrović [36], the magnitude of work required to produce a chip is approximately 10% higher for up milling, since the cutting thickness is higher at the tooth exit. When milling with a depth of cut of 1.5 mm (Fig. 3(d)), the maximum surface temperature was 188°C, which corresponds to an increase of approximately 61% and 23% in relation to the depths of cut of 0.5 and 1.0 mm, respectively. In this case, a higher temperature is observed in regions extending slightly ahead of the cutting zone, due to the increased severity of the operation. It is noteworthy that the axial depth of cut was the parameter that most affected all components of the milling force due to the increase in the shear area and, consequently, generating more heat during the milling operation and resulting in higher temperatures.

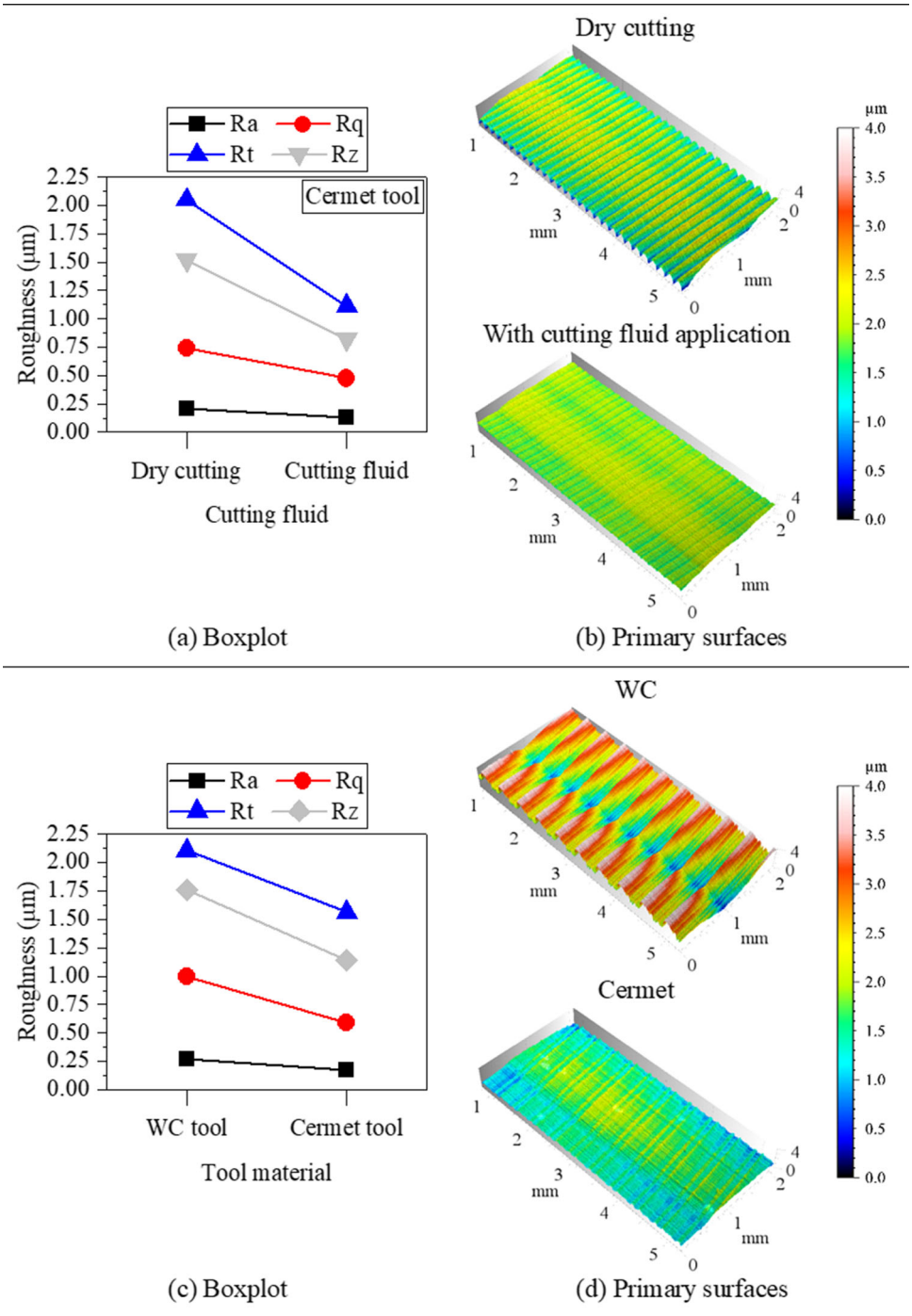

Fig. 5 Influence of the cutting fluid on (a) roughness parameters Ra, Rq, Rz and Rt and (b) Primary surfaces (v_c = 200 mm/min; f_z = 0.05 mm/rev; a_p = 1.5 mm; Tool = cermet) and influence of the tool material on the (c) roughness parameters Ra, Rq, Rz and Rt and (b) primary surfaces (v_c = 100 mm/min; f_z = 0.15 mm/rev; a_p = 0.5 mm; Cutting fluid application)

3.3 Milled surface roughness

Table 2 shows the *p*-values for the roughness parameters Ra, Rq, Rt and Rz for the WC and cermet tools. *P*-values that were statistically significant are shown in bold. For the WC tool, feed per tooth was the only factor that presented a significant effect on all the roughness parameters. For the cermet tool, in addition to the feed per tooth, which significantly influenced the Ra, Rq and Rz parameters, the application of cutting fluid also affected all the roughness parameters. The curvature showed a value above 5% ($p > 0.05$) for all parameters; therefore, it cannot be concluded that any of the factors had a curved relationship with the response, i.e. the mean values of Ra, Rq, Rt and Rz measured at the center point (f_z = 0.10 mm/rev) were not higher or lower than the mean responses for extreme levels of feed per tooth (0.05 and 0.15 mm/rev).

Figure 4(a) shows the influence of feed per tooth and cutting tool grade on the mean values of the roughness parameters Ra, Rq, and Fig. 4(b), Rt and Rz. It can be observed that the higher the feed per tooth, the higher the roughness, especially the Ra and Rt values. This behavior can be explained by the fact that increasing feed leads to the elevation in the distance between adjacent peaks of the roughness profile [37–39]. Figure 4(c) presents images of the primary surfaces to show the effect of increasing feed per tooth from 0.05 to 0.15 mm/rev on the amplitude and geometry of the surface profile generated by milling. As seen previously, the increment of feed per tooth increased Fx, Fy and Fz; therefore, in addition to the geometric effect of the feed per tooth generated by the tool, the influence of elevating the milling force components must be considered, i.e. the inducement of more intense plastic deformation on the workpiece surface during machining that consequently affected roughness parameters [40]. In contrast to feed per tooth (and tool nose radius), which presents as geometric relationship with Ra and Rt, the influence of cutting speed and depth of cut depends on how these parameters affect the milling force components and on the stiffness of the machine tool to bear these forces.

Figure 5 shows the influence of the use of cutting fluid and tool material on the roughness. The application of cutting fluid considerably reduced the average values of the roughness parameters when compared with dry milling (Fig. 5(a)). The cutting fluid plays a key role in reducing friction, since the lubricant film prevents friction between the tool clearance face and the just machined surface, thus reducing roughness, geometric deviations, cutting temperature and tool wear [41]. It is noteworthy that the cutting fluid performed better when cermet inserts were used. According to Klocke [32], the cermet tool, by having high chemical inertness, hardness and oxidation temperature, provides superior performance when compared to WC tool, resulting in surface quality, as seen in Fig. 5(b). Additionally, the better surface quality may be associated with the lower coefficient of friction promoted by cermet at the chip-tool and workpiece-tool interfaces [42].

The average value of the roughness parameters (Ra, Rq, Rt and Rz) generated by the WC inserts are higher than the average values of the roughness parameters generated by the cermet inserts (Fig. 5(c)). As mentioned, cermet has superior properties (chemical inertness, high hardness, oxidation resistance, lower coefficient of friction between the steel-cermet tribological pair) when compared to the WC tool, which improve the tribological behavior of the tool, resulting in higher stability during cutting. In addition, Liu et al. [43] report that cermet has a higher adhesion resistance when compared to WC tool, which results in a better surface finish. The images of the primary surfaces presented in Fig. 5(d) corroborate these results. It is observed that the amplitude of the profiles of the cermet milled surface is much smaller when compared to the WC milled surface, and there is also a modification of the geometric aspect of these profiles.

3.4 Residual stresses

Figure 6 presents the results for residual stresses in the directions parallel ($\sigma_{rs,f}$) and normal ($\sigma_{rs,n}$) to the feed speed as a function of the depth below the surface. In general, tensile residual stresses of low magnitude are induced after milling near the surface (17 μm beneath it). These tensile stresses become zero at a depth of approximately 75 μm and then either stabilize (small fluctuations around zero are due to measurement errors and work material heterogeneity) or are converted to compressive residual stresses at a depth of 75 µm to reach stress values close to zero at a depth of 125 μm. The prevalence of tensile residual stresses on the surface and compressive residual stresses on the subsurface was also identified by Axinte and Dewes [44] when milling AISI H13 steel at high speeds. This fact can be explained by the thermal effects that prevail near the material surface, i.e. temperature rise and thermal expansion on the outer layers of work material. Since the inner layers are not subjected to thermal expansion to the same extent because their temperature is considerably lower, plastic deformation takes place beneath de surface for the sake of material continuity. After machining, temperature decreases and the outer surface layers contraction is hindered by the layers plastically deformed immediately below, thus leading to tensile residual stresses near the surface. In contrast, near-surface compressive residual stresses are observed as the result of mechanical effects: the cutting tool action burnishes the outer layers of the work material and if its yield strength is exceeded, plastic deformation takes place. However, the inner layers are subjected to elastic

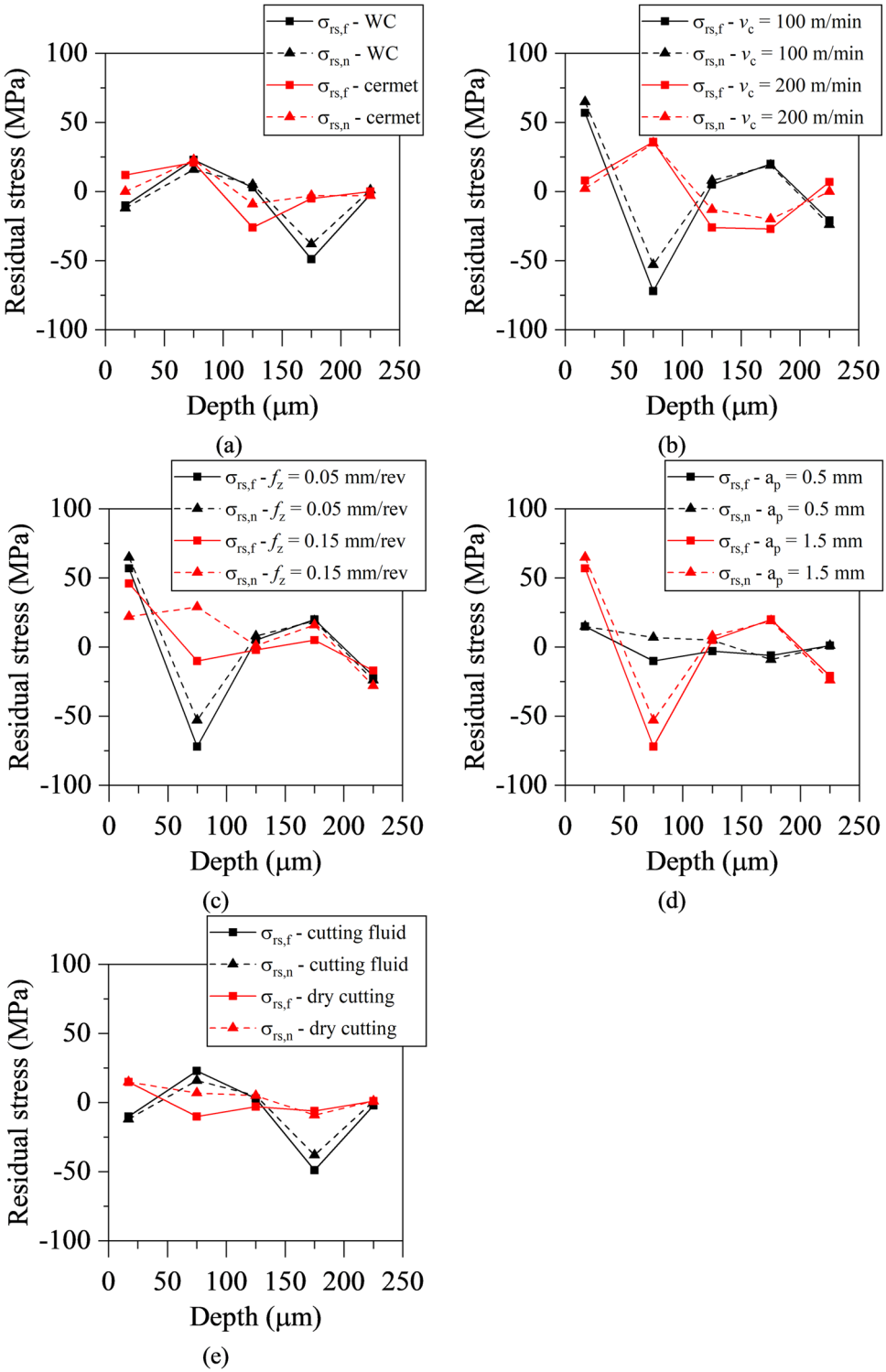

Fig. 6 Influence of (a) tool material, (b) cutting speed, (c) feed per tooth, (d) depth of cut and (e) cutting fluid on residual stresses

deformation and tend to return to their original dimensions after the cutting tool pass, thus promoting compressive residual stresses on the surface layers.

Ma et al. [45] state that thermal effects induce tensile residual stresses and Lin and Chen [46] consider that machining converts power into heat and expansion and contraction phenomena occur in materials. The contraction of the material in the cooling of differently heated and plastically deformed regions during machining represents the main source of residual stresses, since the temperatures

present in the process are of high magnitude, the modulus of elasticity and the yield strength of the metal are drastically reduced, facilitating the flow of the expanding metal.

Figure 6(a) shows that there is no significant difference between the residual stresses induced by WC and cermet inserts. Therefore, the analysis of the effect of the remaining factors on the residual stresses was carried out using WC inserts. The influence of cutting speed on the residual stresses is given in Fig. 6(b). It can be observed that at the depth of 17 μm, the increase in cutting speed reduced the tensile residual stress. Similar results were reported by Zhang, Ding and Li [47]. This effect possibly occurred due to the shorter contact time between the tool and the workpiece at higher cutting speeds, thus minimizing the thermal effects and inducing tensile residual stress of lower intensity near the surface.

The influence of feed per tooth is presented in Fig. 6(c). Near the surface, slightly lower residual stresses were recorded using the highest feed per tooth. This phenomenon can be explained by the mechanical effects of the tool on the machined surface, as the feed per tooth at higher level resulted in higher cutting forces. Thus, the high machining forces may have contributed to plastically deforming the surface of the workpiece, which resulted in tensile residual stresses of lower intensities [15, 40]. Beneath the surface, compressive residual stresses reach a maximum 75 μm for the same reason given above.

Figure 6(d) compares the residual stresses induced by WC inserts when depth of cut is increased from 0.5 to 1.5 mm. It is observed that at the depth of 17 μm the increase in depth of cut induced tensile residual stresses, similar to the results reported by Ji et al. [48]. Increasing depth of cut lead to higher milling forces and temperature on the machined surface. Therefore, this result may be a combination of mechanical effects (generated by the higher feed forces) and thermal effects (generated by the higher temperature of the milled surface). The higher feed forces may have contributed to the plastic deformation near the surface; however, the effect of the higher temperatures may have been predominant in inducing tensile residual stresses of greater intensity. Thus, the increased depth of cut that has been shown to increase the machined surface temperature, induced tensile nature due to the subsequent cooling. The surface machined under high depth of cut may have cooled faster than the subsurface, inducing tensile residual stresses with higher intensities.

The influence of cutting fluid against dry cutting is shown in Fig. 6(e). In contrast to dry cutting, milling with cutting fluid induced compressive residual stress at the depth of 17 μm. The reason for that may be a reduction in the friction coefficient at the tool-workpiece interface. Moreover, the cooling action of the cutting fluid removes heat from the workpiece. Similar results were obtained by Devillez et al. [49].

In general, it was observed that the residual stresses depend on the depth below the surface being analyzed and that opposite effects occurred at depths of 17 μm and 75 μm. Considering that the surface integrity encompasses the surface and the layers immediately beneath it, it can be stated that the analysis at the depth of 17 μm is the most important, mainly because at this depth residual tensile stresses could be detrimental to the fatigue life of the machined part [49]. Thus, aiming machining parameters that minimize tensile residual stresses is a significant contribution of this research. Therefore, it can be concluded that the tensile residual stresses in the layer immediately below the surface is reduced when milling employing higher cutting speed and feed per tooth, lower depth of cut and with the application of cutting fluid, irrespectively of the cutting tool grade.

3.5 Brief results

In the present research, optimal machining conditions are expected to minimize all the investigated responses: milling force components, machined surface roughness, workpiece temperature and tensile residual stresses. The most appropriate way to achieve such goal is to employ multivariate optimization techniques, such as the response surface methodology. Although optimization was not the principal aim of this paper,in general, it can be asserted that the use of cermet inserts with a cutting speed 200 m/min, feed per tooth of 0.05 mm/rev, depth of cut of 0.5 mm in the presence of cutting fluid resulted in the best overall outputs. Finishing milling with cermet inserts is recommended because their superior properties (compared to tungsten carbide) can be effective in minimizing tribological effects on the workpiece material, which tends to reduce roughness and tensile residual stresses. The higher cutting speed is recommended in order to allow higher productivity and tensile residual stresses of lower intensity, since the contact time between the tool and the workpiece is shorter. Lower feed per tooth is recommended to provide better surface finishing and lower depths of cut are recommended to minimize the components of the milling forces, machined surface temperature, and residual stresses. The application of cutting fluid is important to minimize the tribological effects of machining, improving surface quality and reducing tensile residual stresses.

Individually, each input parameter can affect the force components, surface quality and temperature, and residual stresses to a lesser or larger extent. Therefore, it is suitable to establish individual input parameter levels for each output parameter, as shown in Table 3.

Table 3 Recommended milling parameters

	Parameters		
Demand	Output	Input	Recommendation
Cutting force reduction	Milling force	Tool:	WC or cermet
		v_c	Higher
		f_z	Lower
		a_p	Lower
		Cutting fluid	Yes
Surface workpiece temperature reduction	Milled surface temperature	Tool:	WC or cermet
		v_c	Higher
		f_z	Higher
		a_p	Lower
		Cutting fluid	Yes
Surface roughness reduction	Milled surface roughness	Tool:	Cermet
		v_c	Higher
		f_z	Lower
		a_p	Lower or higher
		Cutting fluid	Yes
Reduction of tensile residual stresses near the surface	Residual stresses	Tool:	WC or cermet
		v_c	Higher
		f_z	Higher
		a_p	Lower
		Cutting fluid	Yes

4 Conclusion

In this work, the surface integrity of annealed AISI H13 steel subjected to face milling under various conditions was investigated. The key findings are:

As far as the components of the milling force are concerned, tungsten carbide and cermet tools presented similar results. Depth of cut and feed per tooth were the only statistically significant factors due to their influence on the cutting section area.

Regarding the temperature of the machined surface, the depth of cut was the only significant factor and its increase led to higher temperatures due the higher amount of energy to shear a larger cutting section area.

Concerning the machined surface roughness, increasing feed per tooth resulted in an increase in the roughness parameters due to both the larger distance between adjacent roughness profile peaks and the higher milling forces (higher surface plastic deformation). The application of cutting fluid reduced roughness due to the tribological effect of the lubricating-cooling action in the interface between the tool rake face and the just machined surface. The cermet promoted better surface finish when compared to the WC tool, possibly due to its excellent properties leading to better tribological conditions.

Finally, with regarding to the induced residual stresses, the use of high cutting speed and feed per tooth reduced the tensile residual stresses near the surface. The increase in depth of cut elevated the tensile residual stresses due to the higher temperatures developed, which is directly related to the increase in the components of the milling forces. The application of cutting fluid reduced the intensity of the tensile residual stresses.

Acknowledgements The authors are grateful to the Mechanical Engineering Graduate Program of the University de Minas Gerais and the Brazilian research agency CAPES for financial support.

Funding This study was financed in part by the Coordenação de Aperfeiçoamento de Pessoal de Nível Superior - Brasil (CAPES) - Finance Code 001.

Declarations

Consent to participate All the authors consent to participate in this research.

Consent for publication The authors give full consent to the publisher for the publication of this work.

Competing interests The authors declare no competing interests.

References

1. Jing L, Liu G, Chen M (2006) Study on surface integrity in hard milling of hardened die steel, vol 533, pp 540–543. https://doi.org/10.4028/www.scientific.net/MSF.532-533.540
2. Cheloni JPM, Fonseca EB, Gabriel AHG, Lopes ÉSN (2022) The transient temperature field and microstructural evolution of additively manufactured AISI H13 steel supported by finite element analysis. J Materials Res Technol 19:4583–4597. https://doi.org/10.1016/j.jmrt.2022.06.143
3. Afazov SM, Ratchev SM, Segal J (2012) Prediction and experimental validation of micro-milling cutting forces of AISI H13 steel at hardness between 35 and 60 HRC, pp 887–899. https://doi.org/10.1007/s00170-011-3864-7
4. Rahmati B, Sarhan AAD, Sayuti M (2014) Investigating the optimum molybdenum disulfide (MoS 2) nanolubrication parameters in CNC milling of AL6061-T6 alloy, pp 1143–1155. https://doi.org/10.1007/s00170-013-5334-x
5. Cui X, Zhao J, Jia C, Zhou Y (2012) Surface roughness and chip formation in high-speed face milling AISI H13 steel. Int J Adv Manufacturing Technol 61(1-4):1–13. https://doi.org/10.1007/s00170-011-3684-9
6. Ding T, Zhang S, Wang Y, Zhu X (2010) Empirical models and optimal cutting parameters for cutting forces and surface roughness in hard milling of AISI H13 steel, pp 45–55. https://doi.org/10.1007/s00170-010-2598-2
7. Kant G, Sangwan KS (2014) Prediction and optimization of machining parameters for minimizing power consumption and surface roughness in machining. J Clean Prod 83:151–164. https://doi.org/10.1016/j.jclepro.2014.07.073
8. Do TV, Nguyen QM, Pham MT (2020) Optimization of cutting parameters for improving surface roughness during hard milling of AISI H13 steel. Key Eng Materials 831 KEM, pp 35–39. https://doi.org/10.4028/www.scientific.net/KEM.831.35
9. Jhavar S, Paul CP, Jain NK (2013) Causes of failure and repairing options for dies and molds : a review. Eng Fail Anal 34:519–535. https://doi.org/10.1016/j.engfailanal.2013.09.006
10. Li B, Zhang S, Zhang Q, Chen J, Zhang J (2018) Modelling of phase transformations induced by thermo-mechanical loads considering stress-strain effects in hard milling of AISI H13 steel. Int J Mech Sci 149(October):241–253. https://doi.org/10.1016/j.ijmecsci.2018.10.010
11. Eric M, Nedic B (2002) Materials machinabilitv in relation to the cutting temperature. Tribology Industr 24(3):1–4
12. Armendia M, Garay A, Villar A, Davies MA, Arrazola PJ (2010) CIRP annals - manufacturing technology high bandwidth temperature measurement in interrupted cutting of difficult to machine materials. CIRP Ann Manuf Technol 59(1):97–100. https://doi.org/10.1016/j.cirp.2010.03.059
13. Davies MA, Ueda T, MSaoubi R, Mullany B, Cooke AL (2007) On the measurement of temperature in material removal processes 1, vol 56(2), pp 581–604. https://doi.org/10.1016/j.cirp.2007.10.009
14. Moreira MDO, Abrão AM, Ferreira RAM, Porto MP (2021) International journal of heat and mass transfer temperature monitoring of milling processes using a directional-spectral thermal radiation heat transfer formulation and thermography. Int J Heat Mass Trans 171:121051. https://doi.org/10.1016/j.ijheatmasstransfer.2021.121051
15. Su J-C, Young KA, Ma K (2012) Modeling of residual stresses in milling. Int J Adv Manuf Technol:717–733. https://doi.org/10.1007/s00170-012-4211-3
16. Qehaja N, Doçi I, Bruçi M, Abdullahu F, Jakupi K, Zhujani F (2016) Mathematical modelling of surface roughness through machining parameters and machining time during the dry milling process. Annals DAAAM Proc Int DAAAM Symposium 27(1):187–194. https://doi.org/10.2507/27th.daaam.proceedings.028
17. Shaw MC, Cookson J (2005) Metal cutting principles vol 2. Oxford University Press, New York
18. Aslan E, Camuscu N (2005) A comparative study on cutting tool performance in end milling of AISI D3 tool steel, vol 170, pp 121–126. https://doi.org/10.1016/j.jmatprotec.2005.04.111
19. Ribeiro JLS, Diniz SB, Carlos J, Rubio C, Abrão AM (2012) Dimensional and geometric deviations induced by milling of annealed and hardened AISI H13 tool steel (February 2020), pp 13–21. https://doi.org/10.5923/j.materials.20120201.03
20. Kun H, Wenyu Y (2017) International journal of mechanical sciences analytical analysis of the mechanism of effects of machining parameter and tool parameter on residual stress based on multivariable decoupling method, vol 129, pp 659–679. https://doi.org/10.1016/j.ijmecsci.2017.05.031
21. E837-13a ASTM (2013) Standard test method for determining residual stresses by the Hole-Drilling Strain-Gage method. Standard Test Method E837-13a i, pp 1–16. https://doi.org/10.1520/E0837-13A.2
22. El-Khabeery MM, Fattouh M (1989) Residual stress distribution caused by milling. Int J Mach Tools Manuf 29(3):391–401. https://doi.org/10.1016/0890-6955(89)90008-4
23. Abishekraj N, Gowtham T, Bibeye Jahaziel R, Krishnaraj V, Geetha Priyadarshini B (2021) Investigation of cutting temperature on machining titanium alloys using micro-textured cutting inserts, pp 387–396. https://doi.org/10.1007/978-981-15-9809-8_31
24. Arun Ramnath R, Thyla PR, Mahendra Kumar N, Aravind S (2018) Optimization of machining parameters of composites using multi-attribute decision-making techniques: a review. J Reinf Plast Compos 37(2):77–89. https://doi.org/10.1177/0731684417732840
25. Ramnath RA, Thyla PR (2022) Measurement and optimization of multi-attribute characteristics in milling epoxy granite composites using rsm and combined ahp-topsis surface topography: metrology and properties, vol 10(2). https://doi.org/10.1088/2051-672X/ac4566
26. Gokulkumar S, Thyla PR, ArunRamnath R, Karthi N (2020) Acoustical analysis and drilling process optimization of camellia sinensis / ananas comosus / GFRP / epoxy composites by TOPSIS for indoor applications. J Natural Fibers 18(12):2284–2301. https://doi.org/10.1080/15440478.2020.1726240
27. Arunramnath R, Thyla PR, Mahendrakumar N, Ramesh M, Siddeshwaran A (2019) Multi-attribute optimization of end milling epoxy granite composites using TOPSIS. Mater Manuf Process 34(5):530–543. https://doi.org/10.1080/10426914.2019.1566960
28. Arun Ramnath R, Thyla PR, Harishsharran AKR (2020) Machining parameter selection in milling epoxy granite composites based on AHP. Materials Today Proc 42:319–324. https://doi.org/10.1016/j.matpr.2020.09.340
29. Montegomery D (2013) Design and analysis of experiments - a supplement for using JMP, vol 53, pp 1689–1699
30. Tyssedal J, Samset O (1997) Analysis of the 12 run Plackett-Burman design 1 introduction. Preprint Stat:1–22
31. Vanaja K, Rani RHS (2007) Design of experiments: concept and applications of plackett burman design. Clin Res Regul Aff 24(1):1–23. https://doi.org/10.1080/10601330701220520
32. Klocke F (2011) Manufacturing processes 1: cutting, p 504. Springer. https://doi.org/10.1007/978-3-642-11979-8
33. Çiçek A, Ekici E, Kivak T, Kara F, Uçak N (2021) Performance of multilayer coated and cryo-treated uncoated tools in machining of AISI H13 tool steel—part 2: HSS end mills. J Mater Eng Perform 30(5):3446–3457. https://doi.org/10.1007/s11665-021-05657-9

34. Chuangwen X, Ting X, Xiangbin Y, Jilin Z, Wenli L (2016) Experimental tests and empirical models of the cutting force and surface roughness when cutting 1Cr13 martensitic stainless steel with a coated carbide tool. Adv Mech Eng 8(10):1–10. https://doi.org/10.1177/1687814016673753
35. Yan H, Hua J, Shivpuri R (2005) Numerical simulation of finish hard turning for AISI h13 die steel. Sci Technol Adv Mater 6(5):540–547. https://doi.org/10.1016/j.stam.2005.04.002
36. Tadić B, Marjanović N, Mitrović S (2006) Kinematic, dynamic and tribological aspects of up and down milling processing. Tribology Industr 28(1-2):19–26
37. Davim JP (2018) Surface integrity in machining, pp 10–27
38. Baek DK, Ko TJ, Kim HS (2001) Optimization of feedrate in a face milling operation using a surface roughness model. Int J Mach Tools Manufacture 41(3):451–462. https://doi.org/10.1016/S0890-6955(00)00039-0
39. Qehaja N, Doçi I, Bruçi M, Abdullahu F, Jakupi K, Zhujani F (2016) Mathematical modelling of surface roughness through machining parameters and machining time during the dry milling process. Annals of DAAAM Proc Int DAAAM Symposium 27(1):187–194. https://doi.org/10.2507/27th.daaam.proceedings.028
40. Reimer A, Luo X (2018) Prediction of residual stress in precision milling of AISI h13 steel. Procedia CIRP 71:329–334. https://doi.org/10.1016/j.procir.2018.05.036
41. Manimaran G, Nimel Sworna Ross K (2018) Surface behavior of AISI H13 alloy steel machining under environmentally friendly cryogenic MQL with PVD-coated tool. J Testing Evaluation, vol 48(4). https://doi.org/10.1520/JTE20180130
42. Federici M, Menapace C, Moscatelli A, Gialanella S, Straffelini G (2016) Effect of roughness on the wear behavior of hvof coatings dry sliding against a friction material. Wear 368-369:326–334. https://doi.org/10.1016/j.wear.2016.10.013
43. Liu J, Ji X, Guo Z, Qin C, Xiao Y, You Q (2020) Characteristics and cutting perfomance of the CVD coatings on the tiCN-based cermets in turning hardened AISI H13 steel. J Materials Res Technol 9(2):1389–1399. https://doi.org/10.1016/j.jmrt.2019.11.065
44. Axinte DA, Dewes RC (2002) Surface integrity of hot work tool steel after high speed milling-experimental data and empirical models. J Mater Process Technol 127(3):325–335. https://doi.org/10.1016/S0924-0136(02)00282-0
45. Ma Y, Feng P, Zhang J, Wu Z, Yu D (2016) Prediction of surface residual stress after end milling based on cutting force and temperature. J Mater Process Technol 235:41–48. https://doi.org/10.1016/j.jmatprotec.2016.04.002
46. Lin YC, Chen SC (2003) Effect of residual stress on thermal fatigue in a type 420 martensitic stainless steel weldment. J Mater Process Technol 138(1-3):22–27. https://doi.org/10.1016/S0924-0136(03)00043-8
47. Zhang S, Ding TC, Li JF (2012) Determination of surface and in-depth residual stress distributions induced by hard milling of H13 steel. Production Eng 6(4-5):375–383. https://doi.org/10.1007/s11740-012-0390-x
48. Ji C, Sun S, Lin B, Fei J (2018) Effect of cutting parameters on the residual stress distribution generated by pocket milling of 2219 aluminum alloy. Adv Mech Eng 10(12):1–15. https://doi.org/10.1177/1687814018813055
49. Devillez A, Coz GL, Dominiak S, Dudzinski D (2011) Journal of materials processing technology dry machining of inconel 718 , workpiece surface integrity. J Mater Process Tech 211(10):1590–1598. https://doi.org/10.1016/j.jmatprotec.2011.04.011